KSCE Journal of Civil Engineering (2023) 27(5):2263-2274
DOI 10.1007/s12205-023-1761-x

pISSN 1226-7988, eISSN 1976-3808
www.springer.com/12205

Tunnel Engineering

Study on Assembly and Tensile Performance of Circumferential Anchor Joint for Shield Tunnel Considering Roughness and Size of Structure

Gaole Zhang[a,b], **Wenjun Zhang**[a,b], **Jiahao Li**[b], **Xinnan Zhou**[b], **Wang Liu**[b], **and Jianbing Qi**[b]

[a]*School of Civil Engineering and Architecture, Guangxi University, Nanning 530004, China*
[b]*School of Civil Engineering, Tianjin University, Tianjin 300350, China*

ARTICLE HISTORY

Received 27 September 2022
Revised 27 January 2023
Accepted 10 February 2023
Published Online 19 March 2023

KEYWORDS

Shield tunnel
Segmental joint
Anchor effect
Tensile performance
Assembly behavior

ABSTRACT

Anchor joint is conducive to improving the automation level of the shield tunneling method, whose mechanical behavior is still not fully clear due to the complicated interaction among various structural components. In this paper, a refined FEM model is established and adopted to investigate the anchor joints' assembly and tensile performance. The operation principles of the anchor joint are first introduced for better understanding. Then, a detailed description is presented for the developed refined FEM, including the material properties, structural features, and verification. After that, 76 working conditions in total are set, and an in-depth study is conducted to examine the influence of surface roughness, gap sizes, and strength grades on the assembly and tensile behavior of anchor joints both quantitatively and qualitatively. The results show that the surface roughness mainly influences the maximum assembly load and tensile capacity of anchor joints. The gap size obviously impacts both quantitative and qualitative assembly characteristics and tensile behavior for anchor joints, whose effect is more significant than the surface roughness. The strength grade has a different influence on the distinct mechanical behavior of anchor joints. There is a positive correlation between anchor joints' assembly and tensile behavior. To satisfy the requirement of enough tensile capacity and reasonable assembly difficulty, a good solution should be to reach an appropriate balance between the assembly and tensile behavior of anchor joints.

1. Introduction

The shield tunneling method has gained widespread adoption in the construction of metro lines (Gharehdash and Barzegar, 2015; Lai et al., 2021; EDCJHT, 2022), urban highway projects (Talmon and Bezuijen, 2013), municipal utility tunnels (Kim et al., 2020; Yang et al., 2020), and water conveyance tunnels (Jin et al., 2017), due to its significant advantages of high automation, excellent efficiency, and low environmental disturbance. Using this method, a large number of precast segmental linings are in need to construct the tunnel, and extensive longitudinal and circumferential joints are thus formed. The seismic response of prefabricated underground structures should be more complicated than those of the cast-in-place ones (Tao et al., 2020). According to the existing investigations (Wang et al., 2018a, 2018b; Tan et al., 2020), the segmental joints are most vulnerable to structural damage and leakage failure, which has a direct influence on the reliability and security of the whole tunnel. Therefore, it is of critical importance to reveal the mechanical and waterproof performance of the segmental joints. Generally, the segmental joints should be tightly linked with different types of connectors, among which the bolt has been the most popular and common selection, e.g., short straight bolts, long straight bolts, inclined bolts, and bending bolts (Jin et al., 2018; Wang et al., 2021; Zhang et al., 2021a; Zhang et al., 2022b). It is well known that the static and dynamic performance of segmental joints will show obvious distinctions if different connectors are employed. Hence, it is challenging to reach a universal criterion that can accurately describe the behavior of all the segmental joints with additional features.

There have been many achievements made in research on the weakening effects of joints, including theoretical approaches (Lee and Ge, 2001; Li et al., 2015a, 2015b; Liu et al., 2022), experimental observations (Ding et al., 2013; Liu et al., 2017; Zuo et al., 2018; Tao et al., 2019, 2022b), and numerical solutions

CORRESPONDENCE Wenjun Zhang wjzhang@gxu.edu.cn School of Civil Engineering and Architecture, Guangxi University, Nanning 530004, China; School of Civil Engineering, Tianjin University, Tianjin 300350, China

(Zhang et al., 2021a; Tao et al., 2021, 2022a). For the theoretical methods, the joint effect can be considered by adding a reduction to the bending bearing capacity of the integral tunnel rings (Wood, 1975). Under such conditions, the detailed characteristics of the segmental joints are actually neglected. To better reproduce the actual situations, some publications simplified the joints into springs in various directions (El Naggar and Hinchberger, 2008; Teachavorasinskun and Chub-uppakarn, 2010), namely the so-called beam-spring, shell-spring, and solid-spring models. In this way, the mechanical behavior of the joint can be taken into account both linearly and nonlinearly in the light of the specific requirements (Ding et al., 2013; Jin et la., 2018). The experimental method is another effective approach to examining the mechanical property of the segmental joints. Liu et al. (2017) carried out a series of experiments to obtain the bearing capacity of segmental joints as well as the failure mechanism. Zuo et al. (2018) investigated the mechanical behavior of the longitudinal joints by analyzing the relationship between the joint opening and internal force. Given that the ultimate bearing capacity of the segmental joint connected by simple bolts cannot meet the safety requirements under conditions of big cross-section, large buried depth, and high water table, some novel improvements have been tried on the structure of joints. Zhou et al. (2019, 2022) tested the stiffness of a segmental joint with ductile-iron panels and further explored the detailed damage process of whole lining structures through full-scale experiments. Ding et al. (2021) focused on the static performance of a segmental joint under flexural action. It was found that higher joint stiffness can be gained with double rows of bolts. Additionally, the stress concentration phenomenon is mainly observed around the hand hole areas. Looking at this problem, Wang et al. (2019) executed several model tests to discuss the impact of the hand hole on the bearing capacity and damage features of the joint in shield tunnels. Moreover, the numerical method is also extensively used to evaluate the safety state of the joint and validate the experimental results thanks to its cost-effectiveness and flexibility, especially for the investigations of three-dimensional stress distribution and progressive failure characteristics (Jin et al., 2017; Ding et al., 2021; Zhang et al., 2022a). The above-mentioned reports have made outstanding contributions to the in-depth understanding of the mechanical characteristics of segmental joints, while there is also attention paid to waterproof performance (Zhang et al., 2021b; Zhang et al., 2021c), thermo-mechanical behavior (Shen et al., 2021), and seismic responses (Guo et al., 2021; Liu et al., 2021).

Although there exist numerous valuable references for the comprehensive knowledge of segmental joints, nearly all of the available findings are concentrated on conventional bolt joints. From the past research, it is apparent that the bolt joints have certain limitations despite their reliable strength and extensive application (Liu et al., 2018; Liu et al., 2019). When using bolt joints, it is inevitable to set hand holes, which causes degradation to the overall strength of segments (Chen and Mo, 2009; Wang et al., 2019). Furthermore, local cracks are mainly found near the hand holes, which may further lead to water leakage and sand gushing (Wu et al., 2020). Moreover, the bolt is vulnerable to rust, as it is directly exposed to the air and humid environment. Then, the durability and normal operation of the tunnel lining structures will be adversely affected. Since the bolt joints require a large amount of manual operation, the use of which also brings restrictions on construction efficiency and automation level. Thus, it is necessary to develop and adopt new types of joints for shield tunnels to gain higher resistance and better performance.

In view of the limitations of the bolt joints, various novel joints have been created, such as the anchor joint and CT joint (Nakajima et al., 1998; Shirato et al., 2003), which have the merits of high strength, excellent precision, quick connection, and good automation. Compared with the conventional bolt joints, these newly developed joints can be used without hand holes, thereby successfully eliminating the corresponding weakening impact. Besides, the assembly of the new joints can be easily finished under the jack thrust so that no extra manual operation is required, producing significant savings. However, the newly developed joints are characterized by complicated structures whose mechanical behavior is not very clear. Though the adoption of the new joints can already be found in some tunnel projects, there is still a long way to go before fully understanding the essential design criteria. In addition, the new joints also have more control factors during the application than the bolt joints. Take the anchor joint as an example, since its assembly is completed with the jack thrust, the required force should be less than a certain upper limitation, whereas no similar requirements exist for bolt joints. Consequently, more efforts should be made to interpret the mechanical behavior of the newly developed joints.

This paper aims to conduct investigations on several influence factors of the assembly process and tensile performance of the circumferential anchor joint for shield tunnels. The operation principles of the anchor joint are first introduced as basic information for better understanding. Then, a refined three-dimensional finite element model is established and carefully verified against the experimental results. Using the validated model, further study is carried out to examine the impact of the surface roughness, gap size, and strength specification. The assembly force and tensile bearing capacity are employed as two judgement indicators during the detailed discussions.

2. Overview of Anchor Joint

The anchor joint is developed for the linkage of circumferential joints in shield tunnels. Fig. 1 illustrates the automatic assembly process of the anchor joint under the jack thrust of the shield machine. It can be seen that the progressive assembly of the anchor joint can be easily finished without any other operation except for the jack thrust. Considering the extensive segments needed during the tunnel construction, the increasing efficiency caused by the adoption of anchor joints can lead to significant improvement in automation.

Figure 2 shows an actual scene of the anchor joint in a tunnel project which has already been in service. Just as its name

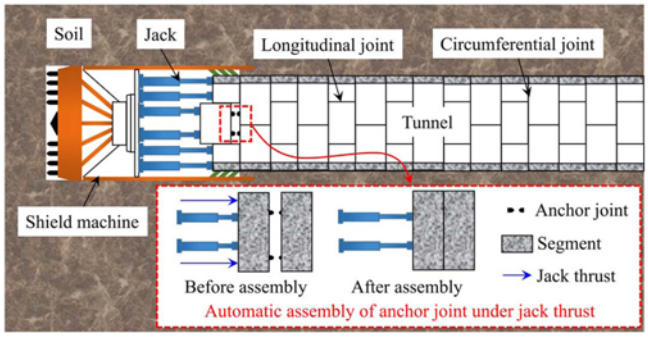

Fig. 1. Automatic Assembly of Anchor Joint under Jack Thrust

implies, the anchor joint consists of several different components, which can be assembled together accompanied by the common segment erection. Three components, i.e., rod, lantern ring, and sleeve, are required to form an anchor joint. When using the anchor joint in a shield tunnel, the three components mentioned above should be cast into the lining structures during the fabrication of the segment. This is quite different from the bolt joints, which also act as a key factor for contributions to the savings of construction. Based on Fig. 2, the sleeve of the anchor joint is generally placed on one lateral surface of the segment, while the lantern ring and rod are set on the opposite lateral surface. With the pressure provided by jack thrust, the circumferential joint opening between the two adjacent segments will be gradually decreased. At the same time, the eight sleeve walls will be forced to deform towards the inside surface of the lantern ring due to the compression from the rod. Finally, the sleeve will be totally inserted into the gap between the rod and the lantern ring. In this way, the anchor joint can be eventually formed as a whole, and the so-called anchor effect will be generated to resist the tensile deformation of the circumferential joint.

Given the afore-said characteristics of the anchor joint, it can be inferred that the local geometric structures and sizes may greatly influence its mechanical behavior, especially for the gap between rod and lantern, which directly impacts the final anchor effect. Therefore, it is essential to conduct investigations on the assembly and tensile performance of the anchor joint.

3. Three-Dimensional Refined Finite Element Method

To determine the influence of different factors on the assembly

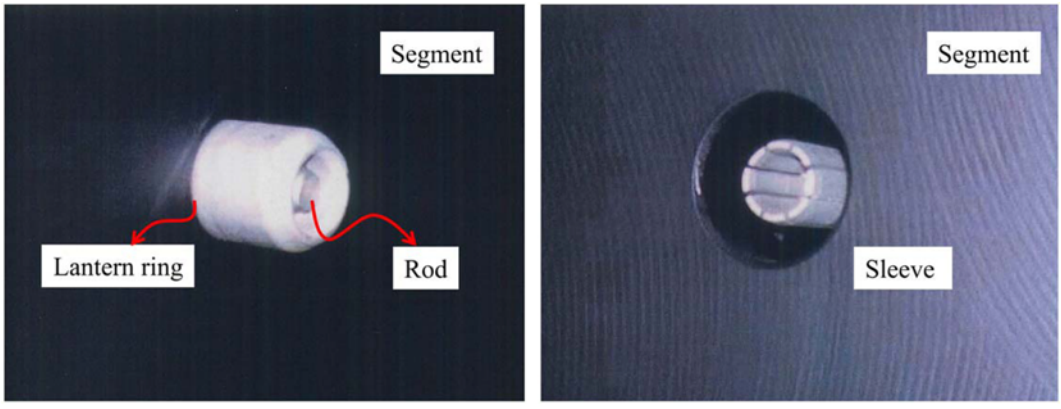

Fig. 2. Real Scene of Anchor Joint: (a) Rod and Lantern Ring, (b) Sleeve

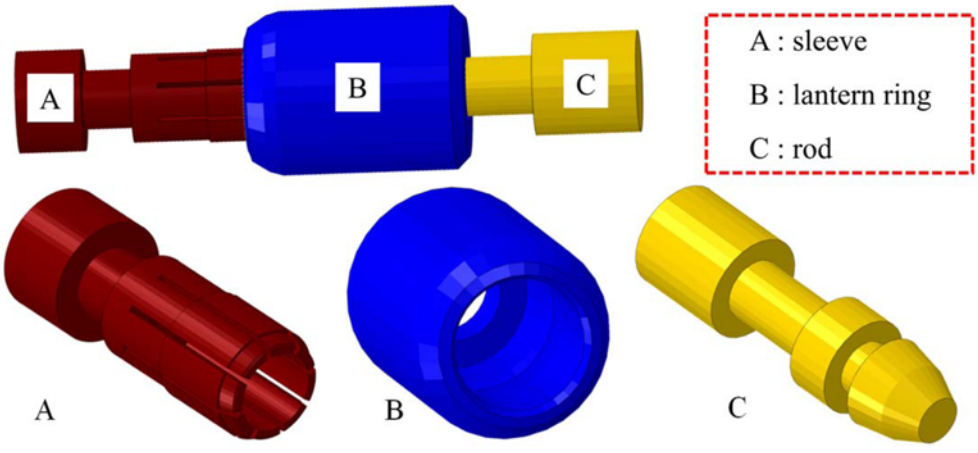

Fig. 3. Numerical Model of Anchor Joint

and tensile performance of the anchor joint, a three-dimensional (3D) refined finite element method (FEM) is adopted in this paper. In this section, the numerical method will be described in detail, including the 3D model of the anchor joint, material properties, contact relationships, boundary conditions, and calibrations of the numerical model.

3.1 Refined Finite Element Model

A refined finite element model is established for the anchor joint, whose dimensions and details are totally the same as the real structures. Fig. 3 displays the 3D numerical model of the anchor joint from whole structures to individual components. The specific dimensions of the anchor joint can be found in the reports published by Nakajima et al. (1998). For simulating the anchor joint, the solid C3D8 element is utilized in this model, and the local mesh refinement is also considered to meet the challenges caused by large deformation.

3.2 Material Properties

During the refined numerical simulation, the elastoplastic double broken line model is selected to reproduce the mechanical behavior of the different metal components included in the anchor joint, as illustrated in Fig. 4. Since the anchor joint is made of ductile-iron materials, the elastic modulus before reaching the yield stress (i.e., E_1) herein is set to be 1.85×10^5 MPa, while the elastic modulus after entering the plastic range (i.e., E_2) is one percent of E_1 (Zhang and Koizumi, 2010). The yield stress is 640 MPa with the use of an 8.8-grate rod, and the Poisson's ratio equals to be 0.27.

3.3 Contact Relationships

Considering the structural characteristics and working mechanism of the anchor joint, it is extremely important to determine reliable contact relationships to reflect the real interaction between different components. For this purpose, the surface-to-surface contact is employed, in which a master surface and a slave surface should be defined for each contact pair, respectively. In addition, the surface-to-surface contact contains two directional attributes, namely the normal and tangential directions. In the normal direction, the hard contact is selected, which takes into account the Lagrange Multipliers to strengthen the contact constraints (Van Nguyen et al., 2017), making the surface-to-surface discretization allowable. While in the tangential direction, the finite sliding approach is used with the penalty function, which can be controlled by a constant friction coefficient. The specific friction coefficient will be fixed through parameter inversion during the model calibrations in the following section.

3.4 Model Calibrations

Before conducting the detailed study, careful verifications should be first finished for the established numerical model to calibrate its effectiveness and reliability. In order to finish this task, the detailed assembly and tensile process of the anchor joint calculated through the refined FEM will be compared with those obtained in the experiments under identical conditions. Based on the model calibrations, the friction coefficient can be reasonably determined.

Nakajima et al. (1998) performed basic tests to gain initial knowledge of the performance of the anchor joint using a simplified setup. As shown in Fig. 5, only the single anchor joint was included in their tests, while the segment was simplified into the bases of rod and sleeve so that the tests can be completed on a relatively small scale. Firstly, the three components contained in an anchor joint were separately placed on the same axis. Then, the anchor joint was assembled together under the action of a vertical cylinder. In this process, a load versus joint deformation relationship curve can be drawn, representing the assembly behavior of the anchor joint. After that, the assembled anchor joint was subjected to tensile action. In this case, the sleeve was gradually separated from the rod and lantern ring, and a new

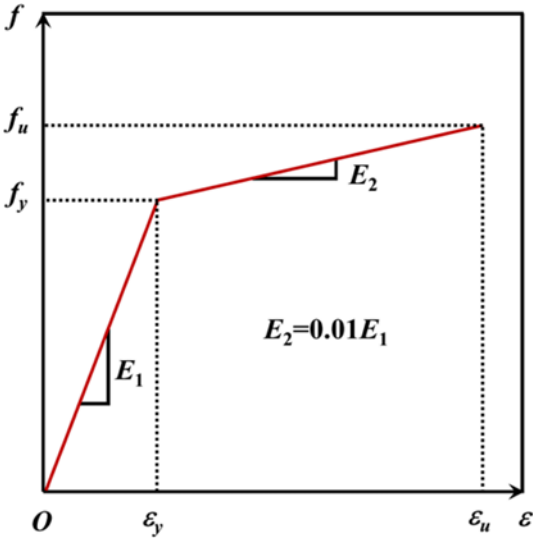

Fig. 4. Elastoplastic Double Broken Line Model for Metal Materials

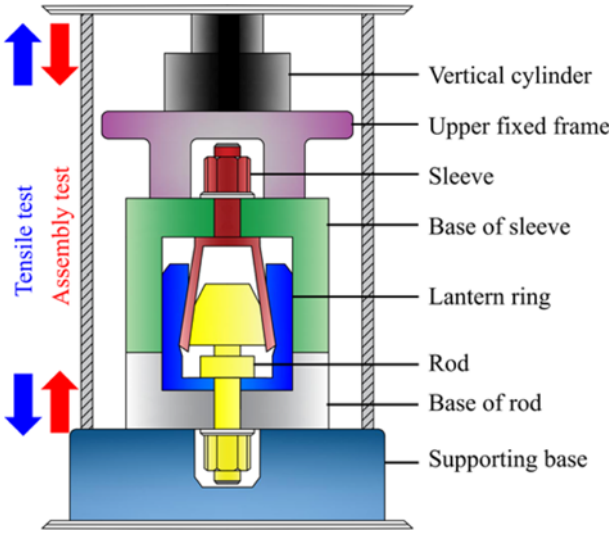

Fig. 5. Assembly and Tensile Tests of Anchor Joint

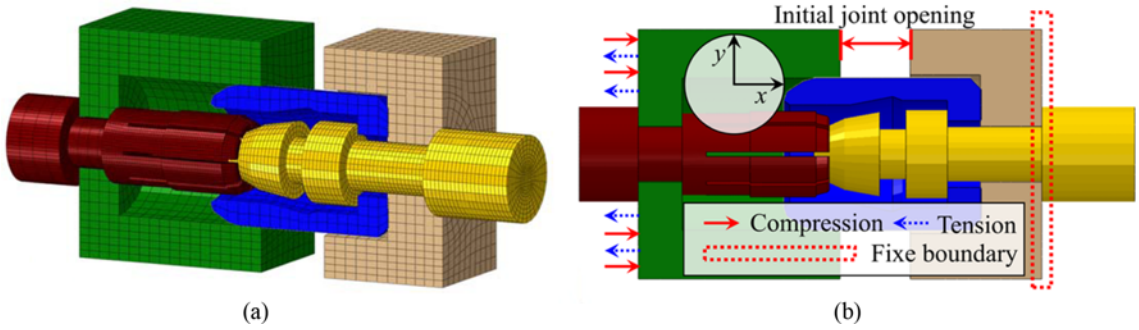

Fig. 6. Verified Model of Anchor Joint: (a) Mesh Results, (b) Load and Boundary Conditions

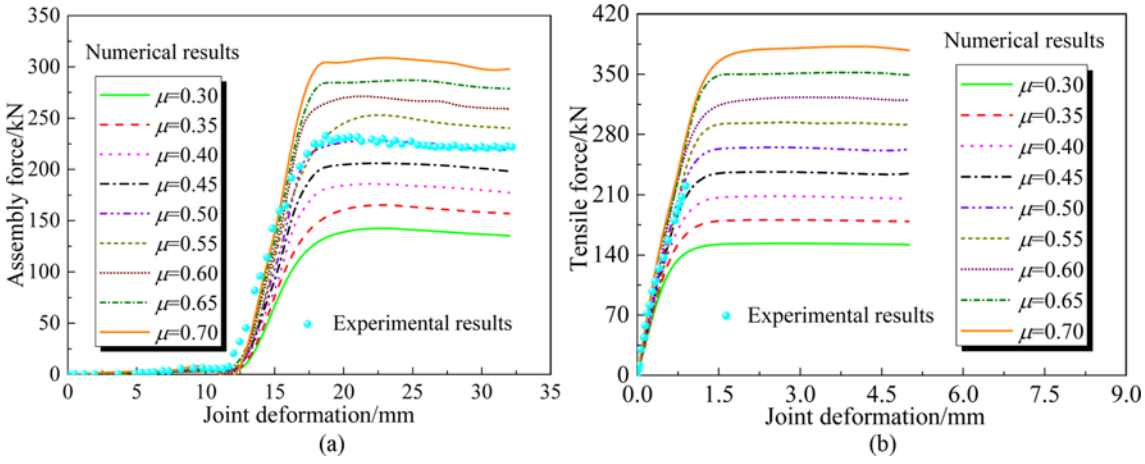

Fig. 7. Comparison between Numerical and Experimental Results: (a) Assembly Process, (b) Tensile Behavior

relationship between the joint opening and necessary load can be obtained.

As mentioned above, the friction coefficient between different components of the anchor joint has a critical impact on the final anchor effect, which plays a vital role in the assembly force and tensile bearing capacity of the anchor joint. Different values were designed to determine the reasonable friction coefficient in the numerical simulation, ranging from 0.3 to 0.7, with an interval of 0.05. Consequently, nine numerical cases were calculated in total, and the corresponding results were compared with those recorded in the experiments. According to the tests shown in Fig. 5, the numerical models of the bases of the rod and sleeve are added, and the verified model is displayed in Fig. 6(a). The solid C3D8 element is used to simulate the bases, and the steel material properties are selected. Hence, the elastic modulus, Passion's ratio, and yield stress of the two base models are 210 GPa, 0.3, and 640 MPa, respectively.

The load and boundary conditions of the verified model for the anchor joint are set as Fig. 6(b) to simulate the experimental conditions. Specifically, the bottom surface of the base of the rod is fixed in three directions, while the displacement load is input on the bottom surface of the base of the sleeve. The assembly force and tensile bearing capacity of the anchor joint can be gained from the reaction force generated at the fixed boundary. It is also worthy of noting that the initial joint opening should be designed as small as possible so that less computational cost is needed. Thus, an initial joint opening of 32 mm is determined, with which the sleeve is just in contact with the rod before the numerical analysis.

The comparison of load versus displacement relationship curves between numerical and experimental results is shown in Fig. 7. It can be seen that the curves of calculation results under different friction coefficient conditions have similar overall characteristics. With the increasing friction coefficient, the maximum assembly force required for the anchor joint assembling continuously increases, while the corresponding tensile bearing capacity experiences simultaneous growth. From the comparison, it is obvious that the numerical results are in good agreement with the experimental results when the friction coefficient is 0.50. Specifically, the key parameters (i.e., compression stiffness, tensile stiffness, peak assembly force, and peak tensile strength) for model calibrations are listed in Table 1. Under the condition with a friction coefficient of 0.50, the error between the experimental and numerical results remains in an acceptable range. Consequently, the above calculation results show that the anchor joint model established in this section is valid and reliable, which can be used to investigate the assembly and tensile performance of anchor joints under other working conditions, and 0.50 should be taken as the reasonable value of friction coefficient for further research.

Table 1. Key Parameters for Model Calibrations

Case	Compression stiffness (kN/mm)	Peak assembly force (kN)	Tensile stiffness (kN/mm)	Peak tensile force (kN)
FEM–μ=0.30	26	140.29	152	153.37
FEM–μ=0.35	30	162.39	181	181.15
FEM–μ=0.40	32	183.42	206	208.79
FEM–μ=0.45	35	204.72	236	237.19
FEM–μ=0.50	**39**	**225.77**	**264**	266.13
FEM–μ=0.55	43	247.49	295	294.93
FEM–μ=0.60	46	266.17	323	323.50
FEM–μ=0.65	50	286.58	352	353.11
FEM–μ=0.70	53	308.08	382	384.28
Experiment	**37**	**231.37**	**259**	-

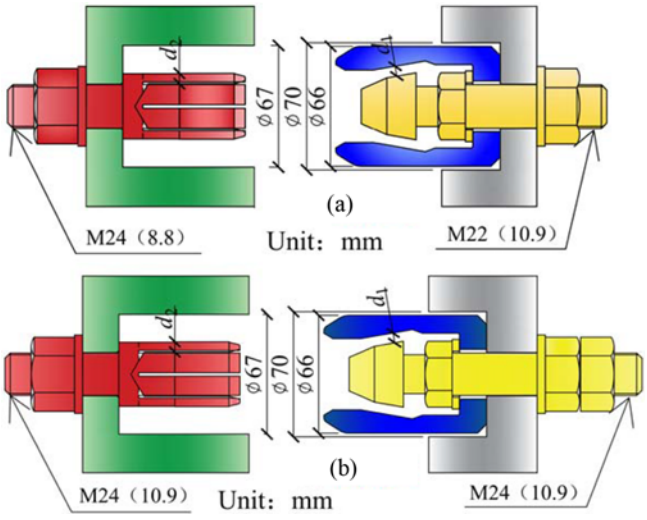

Fig. 8. Anchor Joints with Different Strength Grades: (a) Grade A, (b) Grade B

4. Assembly Behavior of Anchor Joint

In this section, the performance characteristics of the anchor joint during the assembling process will be investigated to reveal the impact of three different factors, including the roughness of the structural surface (i.e., friction coefficient), gap size (Dd = d_2 – d_1, shown in Fig. 8), and strength grade. With this regard, 1) different friction coefficients are set, ranging from 0.45 to 0.55 with an interval of 0.01, 2) 7 distinct gap sizes are determined, ranging from -0.30 to 0.30 with an interval of 0.10, 3) 2 different groups consisting of structures with various strength grades are set as illustrated in Fig. 8. That is, 34 working conditions in total are set to be calculated and discussed.

4.1 Assembly Behavior of Anchor Joint with Different Surface Roughness

For the anchor joint, the friction force generated from the interaction between the sleeve, lantern ring, and rod accounts for a considerable proportion in the assembly performance, which is determined by the surface roughness. Hence, it is of fundamental importance to investigate the influence of surface roughness on the assembly behavior of anchor joints. As described in Section 3.4, the friction coefficient should be 0.5 under the usual conditions. In this regard, different friction coefficients ranging from 0.45 to 0.55 with an interval of 0.01 are set to represent distinct conditions of surface roughness, which may be caused by the possible manufacturing error.

Figure 9 displays the load versus deformation relationship curves obtained during the assembly procedure of anchor joints with strength grade A and B, respectively. From Fig. 9(a), it can be seen that for the anchor joint with strength grade A, the assembly load required in such condition is very small at the beginning of deformation, and this stage continues until the pressing amount reaches about 12 mm. In this stage, the maximum assembly load is less than 5 kN, which can be almost negligible. Then, the required load for the anchor joint assembling increases rapidly, reaching the maximum value at approximately 18 mm. For the second stage with rapid increasing load, the contact extrusion

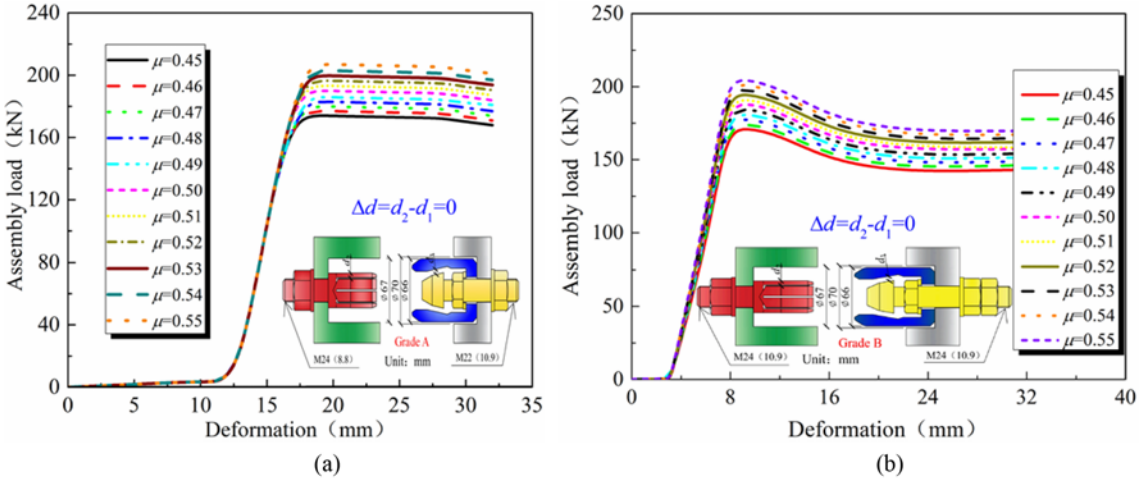

Fig. 9. Assembly Load versus Deformation Relationship with Different Surface Roughness: (a) Grade A, (b) Grade B

and friction between the rod and the sleeve become more and more significant, making the resistance to assembly get greater and greater. After that, the assembly load remains basically unchanged until the deformation reaches about 32 mm, and the anchor joint is totally assembled together. With different surface roughness, it is obvious that the overall characteristics of the assembly behavior of the anchor joint remains nearly identical, except for the maximum value. This may be attributed to that the variation of surface roughness has little influence on the interaction mode among the different structural components of the anchor joint. Specifically, the peak value of the assembly load of the anchor joint with a friction coefficient of 0.45 is approximately 174 kN, while that with a friction coefficient of 0.55 is approximately 207 kN. That is, per increase of 0.01 in the friction coefficient corresponds to the growth of about 3 kN in the peak assembly value. In a word, the friction coefficient has a relatively limited impact on the assembly behavior of the anchor joint, only if it does not experience too much change. Accordingly, the surface roughness should be carefully guaranteed during manufacture so that the peak load of the assembly of the anchor joint can be stable.

On the other hand, the assembly performance of the anchor joint with strength grade B is illustrated in Fig. 9(b). Compared with Fig. 9(a), the overall characteristics of the load-deformation curves show different features, which can be divided into four different stages instead of three stages. In the first stage, the assembly load is quite small before the deformation reaches approximately 3 mm. Then, the assembly load rapidly increases until reaching approximately 8 mm. After that, the assembly load gradually decreases in the third stage, namely from approximately 8 mm to 20 mm. At last, the load remains stable until finishing the total assembly procedure. On the whole, the first stage in the assembly process of anchor joint with strength grade B is shorter than that with strength grade A, while no obvious descent can be observed after reaching the peak assembly load in Fig. 9(a). The difference mentioned above should be caused by the change of strength grade and the corresponding local structural details, which greatly influence the interaction mode among the components of the anchor joint. It is worth noting that a similar correlation can be found between the maximum value of assembly load and the friction coefficient by comparing Figs. 9(a) and 9(b). This phenomenon indicates that the strength grade should be irrelevant to the impact of surface roughness on the assembly behavior of the anchor joint.

4.2 Assembly Behavior of Anchor Joint with Different Gap Sizes

The gap size is another critical parameter determining the assembly behavior of the anchor joint, which has a crucial impact on the interaction mode among the sleeve, rod, and lantern ring. Fig. 10 shows the assembly load versus deformation relationship curves for anchor joints with different gap sizes under conditions of strength grade A and B, respectively. For the anchor joint with strength grade A, it is found that the change of assembly load experiences a similar variation trend. No matter how the gap size changes, the whole relationship curve can be divided into three stages, which is identical to that observed in Section 4.1. Furthermore, the general characteristics of the first and second stages in Fig. 10(a) are in good agreement with those in Fig. 9(a). Nevertheless, the third stage exhibits various variation trends in the light of different gap sizes. That is, when Dd is less than 0, the assembly load tends to decrease, while it keeps unchanged when Dd is greater than 0. It seems that Dd = 0 should be the boundary to distinguish the different performances in the third stages described above. If Dd is less than 0, the interaction acts only between the rod and sleeve during the assembly of the anchor joint, whereas a greater Dd means that the extrusion will appear among more structures, namely the lantern ring. Thus, it is evident that the interaction mode changes with different Dd, resulting in distinct assembly behavior in the third stage. Additionally, compared with the Dd of 0, the peak assembly load of the anchor joint with the Dd of 0.1 mm becomes evidently larger, while that with the Dd of -0.1 mm shows a relatively small decrease. This difference in the change of maximum value for assembly load demonstrates that the manufacturing error

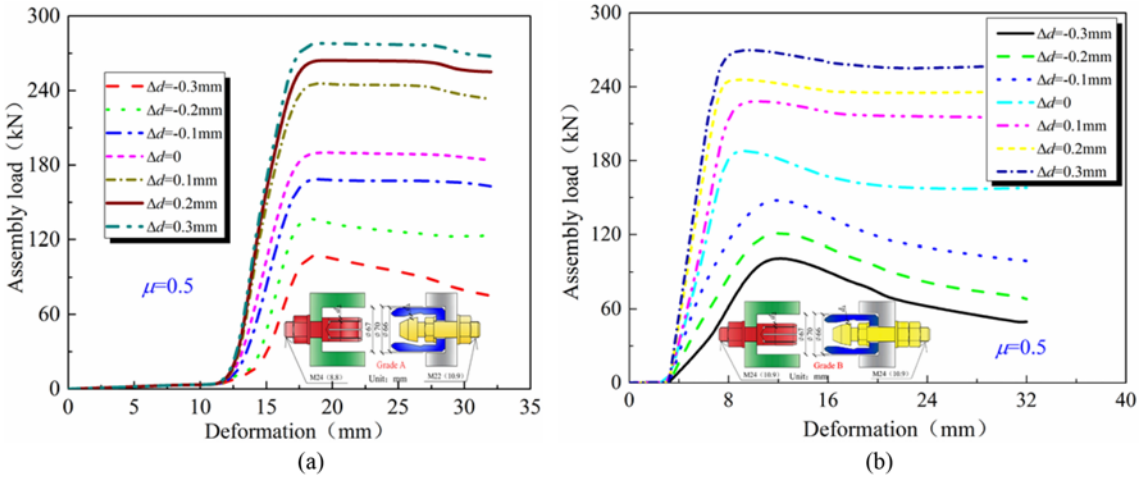

Fig. 10. Assembly Load versus Deformation Relationship with Different Gap Sizes: (a) Grade A, (b) Grade B

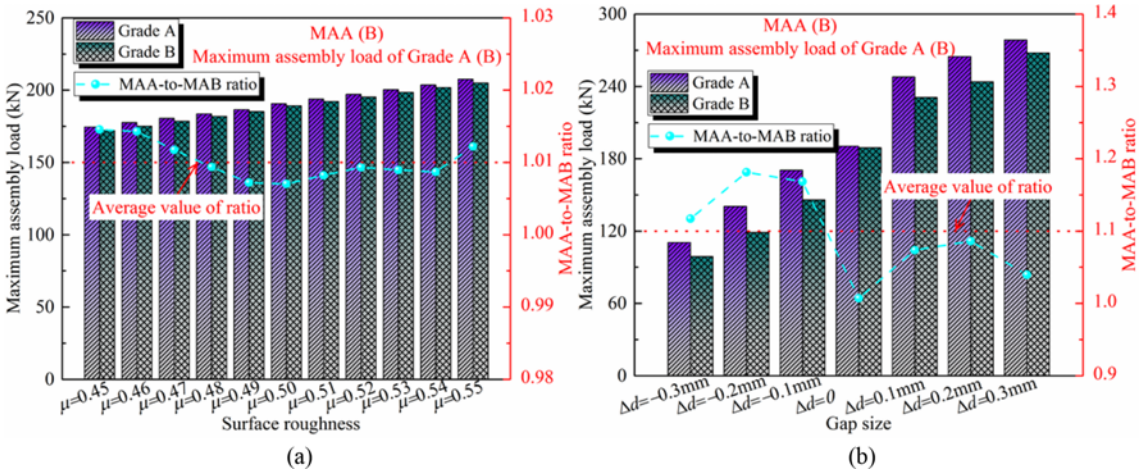

Fig. 11. Assembly Load versus Deformation Relationship with Different Strength Grade: (a) Under Conditions of Different Surface Roughness, (b) under Conditions of Different Gap Sizes

must be treated cautiously, especially for the conditions in which the D*d* is made greater. As the assembly load will rapidly increase in such situations, it can lead to more serious difficulties in overcoming the resistance to installing the anchor joint.

For the anchor joint with strength grade B in Fig. 10(b), it can be seen that the overall characteristics of the load versus deformation curves can be divided into two types, taking the D*d* = 0 as the boundary. Four stages can be observed when D*d* is no less than 0, while only three stages can be found in the other conditions. Moreover, the assembly load reaches the maximum value at approximately 8mm under the conditions in which D*d* is greater than 0, staying the same as those described in Section 4.1. However, for those with a D*d* less than 0, the peak load appears until about 12 mm. Consequently, the required deformation to obtain the maximum value of assembly load increases by about 50% with the decreasing D*d*. Noticeably, the variation in the required deformation found in Fig. 10(b) is not available in Fig. 10(a). That is, the changing gap size can lead to a different variation of assembly behavior according to the corresponding strength grades, which are accompanied by slightly distinct local structural details. Besides, it can be initially inferred that the gap size has a greater effect on changing the assembly behavior than the surface roughness, as no such changes can be found in Fig. 9. Given that the anchor joint has a rather complicated structural feature, more efforts are still in need to fully real the impact of local sizes on its mechanical performance.

4.3 Assembly Behavior of Anchor Joint with Different Strength Grades

Based on the discussions presented in the above two sections, a primary conclusion can be drawn that the strength grade has a particular influence on the assembly behavior of the anchor joint. Since the impact of strength grade has been analyzed in a qualitative way, this section aims to obtain a more detailed correlation between the assembly performances of anchor joints with different strength grades from the aspect of quantification. Considering the fact that the peak assembly load required for installing the anchor joint is the most concerning indicator, it is selected as the parameter to investigate the quantitative relationship.

Figure 11 shows the comparison of the maximum assembly load of anchor joints with different strength grades under the conditions of distinct surface roughness and gap sizes, respectively. The MAA-to-MAB ratio is defined here to facilitate the comparison. It can be observed from Fig. 11(a) that the MAA-to-MAB ratio ranges from 1.005 to 1.015 with the changing surface roughness, and the mean value of the MAA-to-MAB ratio is 1.01. Likewise, under the conditions of different gap sizes, the MAA-to-MAB ratio ranges from 1.0 to 1.2, and the average value of the MAA-to-MAB ratio is 1.1. Combing the correlation features found in Figs. 11(a) and 11(b), it can be preliminarily confirmed that there is a certain relationship available for describing the peak assembly load of anchor joints with different strength grades. Besides, the MAA-to-MAB ratio seems to fluctuate greater with the changing gap sizes than with the variation of surface roughness, which once more provides evidence that the gap size may have a more obvious impact on the assembly behavior of anchor joints. In addition, the difference in the MAA-to-MAB ratio found in Figs. 11(a) and 11(b) implies that the strength grade should be treated as a composite influencing factor for the assembly behavior, which is in need of the consideration of other changing parameters such as the surface roughness and gap sizes, instead of a single one.

5. Tensile Performance of Anchor Joint

Similar to the research on assembly behavior, 38 working conditions in total are determined to investigate the tensile performance of anchor joints.

5.1 Tensile Performance of Anchor Joint with Different Surface Roughness

Figure 12 illustrates the tensile performance of anchor joints with

different surface roughness. The criteria for evaluation of the bearing capacity of anchor joint is the performance characteristics in the extent of a joint opening of 3 mm, which is set to be the maximum value of joint opening focused on in this section.

Compared with the assembly process, the load-displacement curves of the anchor joint with strength grade A in the tensioning process are obviously different, as shown in Fig. 12(a). It can be seen that the tensile bearing capacity directly enters the rising stage from the beginning of joint opening, and reaches the maximum value at about 1.2 mm. After that, the tensile capacity provided by the anchor joint develops slowly and keeps in a stable state. Hence, it can be concluded that the anchor joint has an excellent fastening effect, which can immediately produce resistance under the condition of tension load. In addition, under the same conditions, the fastening force provided by the anchor joint is greater than the required assembly load. This is because the main interaction effect in the assembly process of anchor joints is the mutual extrusion between sleeve and rod, while the lantern ring participates in the mechanical engagement during tensioning so that the anchor joints can provide a higher reverse load. That is, excellent tensile capacity can be obtained for anchor joints with a relatively lower assembly resistance, which indicates that a satisfactory fastening effect is available without too much assembly difficulty.

Figure 12(b) displays the influence of surface roughness on the tensile performance of anchor joints with strength grade B. Comparing Figs. 12(b) with 12(a), it is found that the overall characteristics of the load-displacement curves are nearly identical, which is different from that observed in Section 4.1. Hence, the changing strength grades may only have an impact on the variation trend of the assembly process, but have little influence on the tensile process. Besides, the initial tensile stiffness remains unchanged with the increasing friction coefficient in both Fig. 12(a) and 12(b). This demonstrates that the main effect of surface roughness should be changing the peak tensile capacity.

5.2 Tensile Performance of Anchor Joint with Different Gap Sizes

Figure 13 shows the tensile performance of anchor joints with different gap sizes. The variation trend of the load to joint

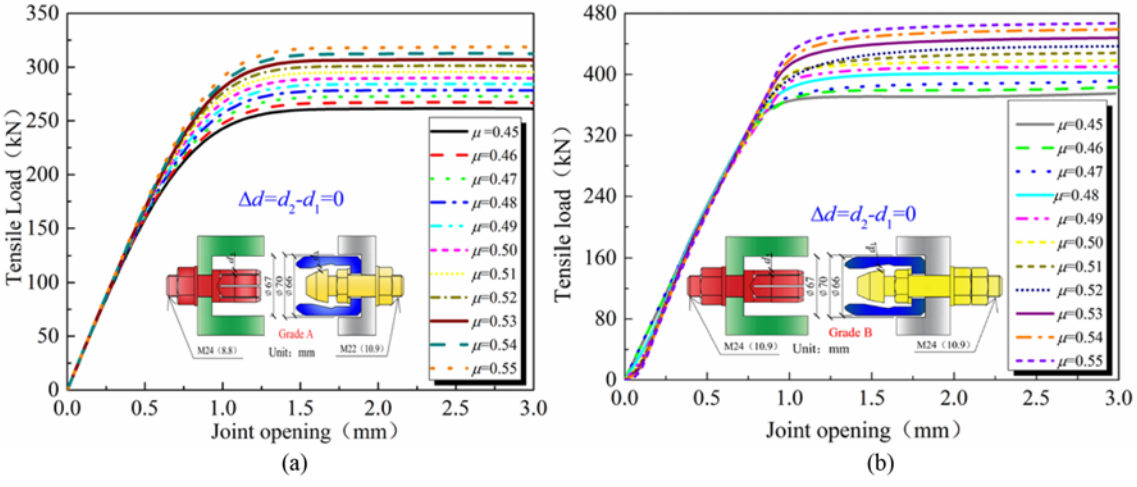

Fig. 12. Tensile Load versus Joint Opening Relationship with Different Surface Roughness: (a) Grade A, (b) Grade B

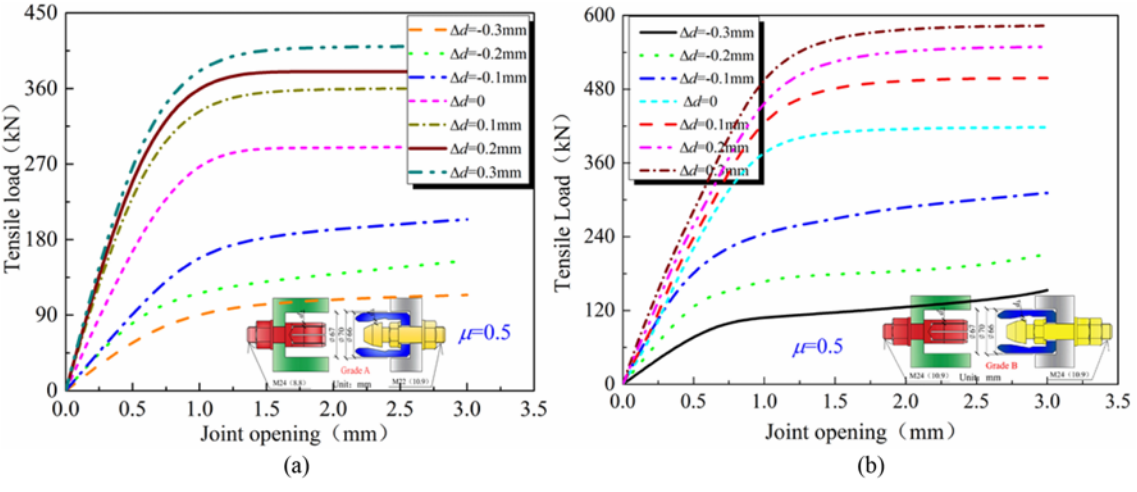

Fig. 13. Tensile Load versus Joint Opening Relationship with Different Gap Sizes: (a) Grade A, (b) Grade B

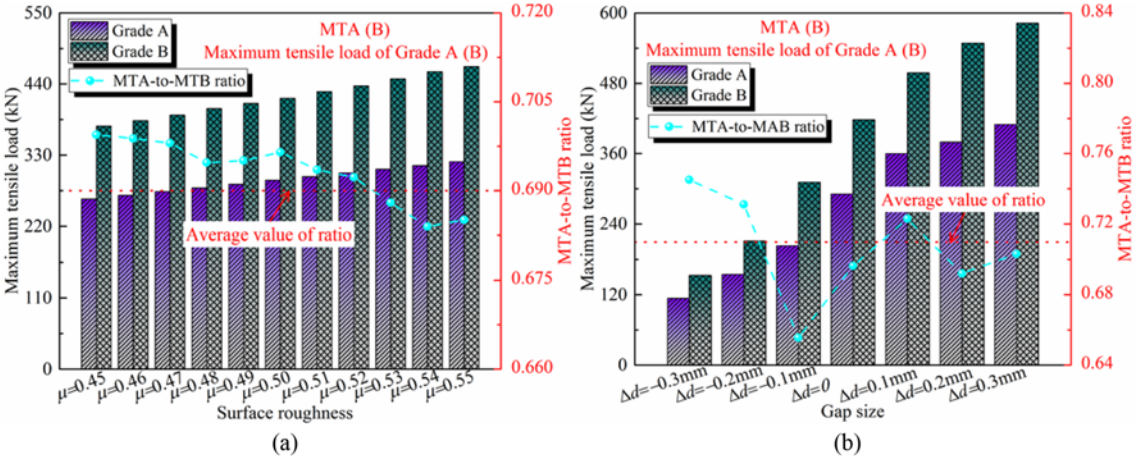

Fig. 14. Tensile Load versus Joint Opening Relationship with Different Strength Grade: (a) Under Conditions of Different Surface Roughness, (b) Under Conditions of Different Gap Sizes

opening curves is similar to that observed in Section 5.1, whereas some differences can also be found for the conditions with a D*d* less than 0. In such conditions, the tensile load increases rapidly in the first stage, and keeps gradually rising in the second stage in both Figs. 13(a) and 13(b), which is different from those with a D*d* greater than 0. This may be caused by the different interaction modes among the components with different gap sizes. Taking the corresponding installation procedure as a comparison, it seems that the increasing process of tensile load in the second stage in Fig. 13 is just similarly opposite to the decreasing process of assembly force in the third stage in Fig. 10. Furthermore, the difference between the maximum tensile load of anchor joints with a D*d* greater than 0 is smaller than that of anchor joints with a D*d* less than 0. This is identical to the difference found in the assembly behavior of anchor joints. Therefore, it can be drawn that there is a specific correlation between the assembly and tensile behavior of anchor joints. Based on the findings in this paper, the tensile capacity of anchor joints will generally show an increasing trend with the growing peak assembly load. To gain outstanding tensile performance, it is better to raise the maximum assembly load to get the corresponding higher bearing capacity, while significant difficulty may appear with too much resistance to finish the installation. Consequently, a good solution is to seek a balance between assembly and tensile performance.

5.3 Tensile Performance of Anchor Joint with Different Strength Grades

It is obvious that the strength grade has a great influence on the tensile performance of anchor joints. However, different from the assembly behavior, the tensile performance of anchor joins with two strength grades shows almost consistent qualitative characteristics. Thus, it is of significant necessity to conduct further quantitative analysis to determine the impact of the strength grade. For this purpose, the MTA-to-MTB ratio, representing the ratio of the maximum tensile load with strength grade A to the maximum tensile load with strength grade B, is defined as the indicator of quantitative analysis.

Figure 14 shows the comparison of the tensile capacity of anchor joints with different strength grades under the conditions of distinct surface roughness and gap sizes, respectively. Based on Fig. 14(a), it can be seen that the MTA-to-MTB ratio ranges from 0.675 to 0.705 with the changing surface roughness, and the mean value is 0.69. Similarly, the MTA-to-MTB ratio ranges from 0.64 to 0.76 with the variation in gap sizes, and the average value ratio is 0.71. The mean value of the MTA-to-MTB ratio obtained from Fig. 14(a) and 14(b) is well agreed with each other, providing confidence that a specific quantitative correlation does exist between the strength grade of the anchor joint and the corresponding tensile performance. Furthermore, the MTA-to-MTB ratio in Fig. 14(b) shows larger fluctuation than that in Fig. 14(a), indicating that the gap size can make a greater impact on the tensile behavior of anchor joints than the surface roughness, which is consistent with that found for the assembly performance. Another interesting phenomenon to be noted is that the strength of grade A and B is 8.8 and 10.9, respectively, whose ratio is also 0.71, nearly the same as the mean MTA-to-MTB ratio gained from Figs. 14 (a) and 14(b). From this point of view, an exciting conclusion can be preliminarily drawn that the material properties have a relatively certain quantitative relationship with the tensile capacity of the anchor joint, despite its complicated structural components. For more rigorous conclusions, a further parametric study is still required with the consideration of other factors and their impacts on the shear performance of anchor joints.

6. Conclusions

In this paper, the assembly and tensile performance of anchor joints with complicated structural features have been investigated, considering the influences of surface roughness, gap sizes, and strength grades, both quantitatively and qualitatively. The detailed conclusions are as follows.

1. The surface roughness mainly influences the maximum assembly load and tensile capacity of anchor joints, while it has little influence on the overall characteristics of the corresponding variation trends and tensile stiffness. The

assembly and tensile load can be increased by raising the surface roughness.

2. The gap size has an obvious impact on both quantitative and qualitative characteristics of assembly and tensile behavior for anchor joints, whose effect is greater than the surface roughness. The boundary to distinguish the different mechanical performances of anchor joints caused by the changing gap size should be Dd = 0, which controls the interaction mode among the sleeve, rod, and lantern ring.
3. The strength grade has a different influence on the distinct mechanical behavior of anchor joints. For the assembly process, the features of load versus deformation curves display apparent changes, while the peak load is nearly the same. For the tensile process, the overall characteristics of variation trends remain in good agreement, whereas the tensile capacity largely grows with increasing strength.
4. There is a positive correlation between the assembly and tensile behavior of anchor joints. The tensile properties of anchor joints will undoubtedly be enhanced when increasing the assembly force. However, combing the requirement of sufficient tensile capacity and controlling the installation difficulty, it is of great importance to seek a reasonable balance between the assembly and tensile behavior of anchor joints.

This paper preliminarily studied the assembly and tensile performance of anchor joint considering the effect of surface roughness and size of the structure. However, there should be more influencing factors which may have significant impacts on the mechanical behavior of anchor joint, due to the corresponding complicated structural features. Additionally, the shear performance is also a critical key for the application of anchor joint, whereas it is not included in this study. Thus, further investigations are still in need for better understanding of the anchor joint's performance, and the foresaid contents will be the future work.

Acknowledgments

The research in this paper was funded by the National Natural Science Foundation of China (Grant No. 51978460), which is gratefully acknowledged.

ORCID

Gaole Zhang https://orcid.org/0000-0001-6533-3437
Wenjun Zhang https://orcid.org/0000-0003-3548-7384

References

Chen J, Mo H (2009) Numerical study on crack problems in segments of shield tunnel using finite element method. *Tunnelling and Underground Space Technology* 24(1):91-102, DOI: 10.1016/j.tust.2008.05.007

Ding P, Tao L, Yang X, Zhao J, Shi C (2019) Three-dimensional dynamic response analysis of a single-ring sructure in a prefabricated subway station. *Sustainable Cities and Society* 45:271-286, DOI: 10.1016/j.scs.2018.11.010

Ding W, Chen X, Jin Y, Qiao Y (2021) Flexural behavior of segmental joint containing double rows of bolts: Experiment and simulation. *Tunnelling and Underground Space Technology* 112(45):103940, DOI: 10.1016/j.tust.2021.103940

Ding W, Peng Y, Yan Z, Shen B, Zhu H, Wei X (2013) Full-scale testing and modeling of the mechanical behavior of shield TBM tunnel joints. *Structural Engineering and Mechanics* 45(3):337-354, DOI: 10.12989/sem.2013.45.3.337

Editorial Department of China Journal of Highway and Transport (EDCJHT) (2022) Review on China's traffic tunnel engineering research 2022. *China Journal of Highway and Transport* 35:1-40, DOI: 10.19721/j.cnki.1001-7372.2022.04.001 (in Chinese)

El Naggar H, Hinchberger SD (2008) An analytical solution for jointed tunnel linings in elastic soil or rock. *Canadian Geotechnical Journal* 45(11):1572-1593, DOI: 10.1139/T08-075

Gharehdash S, Barzegar M (2015) Numerical modeling of the dynamic behaviour of tunnel lining in shield tunneling. *KSCE Journal of Civil Engineering* 19(6):1626-1636, DOI: 10.1007/s12205-015-0406-0

Guo X, Geng P, Wang Q, Chen C, Tang R, Yang Q (2021) Full-scale test on seismic performance of circumferential joint of shield-driven tunnel. *Soil Dynamics and Earthquake Engineering* 151:106957, DOI: 10.1016/j.soildyn.2021.106957

Jin Y, Ding W, Yan Z, Soga K, Li Z (2017) Experimental investigation of the nonlinear behavior of segmental joints in a water-conveyance tunnel. *Tunnelling and Underground Space Technology* 68:153-166, DOI: 10.1016/j.tust.2017.05.018

Jin H, Yu S, Zhou S, Xiao J (2018) Research on mechanics of longitudinal joint in shield tunnel by the nonlinear spring equivalent method. *KSCE Journal of Civil Engineering* 23(2):902-913, DOI: 10.1007/s12205-018-0667-5

Kim K, Kim J, Ryu H, Rehman H, Jafri TH, Yoo H, Ha S (2020) Estimation method for TBM cutterhead drive design based on full-scale tunneling tests for application in utility tunnels. *Applied sciences* 10(15):5187, DOI: 10.3390/app10155187

Lai H, Wang T, Kang Z, Chen R, Hong Q (2021) Theoretical method of chamber pressure for EPB shield tunneling under-crossing existing metro tunnels. *KSCE Journal of Civil Engineering* 25(7):2725-2736, DOI: 10.1007/s12205-021-0755-9

Lee KM, Ge XW (2001) The equivalence of a jointed shield-driven tunnel lining to a continuous ring structure. *Canadian Geotechnical Journal* 38(3):461-483, DOI: 10.1139/t00-107

Li Z, Soga K, Wright P (2015a) Behaviour of cast-iron bolted tunnels and their modelling. *Tunnelling and Underground Space Technology* 50:250-269, DOI: 10.1016/j.tust.2015.07.015

Li X, Yan Z, Wang Z, Zhu H (2015b) Experimental and analytical study on longitudinal joint opening of concrete segmental lining. *Tunnelling and Underground Space Technology* 46:52-63, DOI: 10.1016/j.tust.2014.11.002

Liu X, Li H, Cao W (2018) Comparative experimental study on bending resistance of a new type longitudinal joint connector in shield tunnelling. *Modern Tunnelling Technology* 55(S2):1058-1068, DOI: 10.13807/j.cnki.mtt.2018.S2.137 (in Chinese)

Liu X, Li H, Guan P, Yang Z (2019) Research on design parameters for shield tunnel lining structure with quick connectors. *Modern Tunnelling Technology* 56(6):19-26, DOI: 10.13807/j.cnki.mtt.2019.06.003 (in Chinese)

Liu J, Yuen K, Ke J, Chen W (2022) Developing a prediction model for segment joint opening in an underwater shield tunnel. *Marine Georesources & Geotechnology*, DOI: 10.1080/1064119X.2021.

2017528
Liu Y, Zhang M, Li P, Wang B, Wang L, Yuan P (2021) Experiments on the seismic performance of Y-shape joints of subway stations built by enlarging two parallel shield tunnels. *Tunnelling and Underground Space Technology* 115:104048, DOI: 10.1016/j.tust.2021.104048
Liu X, Zhang C, Zhang C, Yuan Y (2017) Ultimate load-carrying capacity of the longitudinal joints in segmental tunnel linings. *Structural Concrete* 18(5):693-709, DOI: 10.1002/suco.201600070
Nakajima S, Akiyama S, Yasaka M, Sato H, Mukuno K (1998) Development of the axial-slide ductile segment. *Journal of JSCE* 8:39-46 (in Japanese)
Shen Y, Zhu H, Yan Z, Zhou L, Lu Y (2021) Semi-analytical thermo-mechanical model for the shield tunnel segmental joint subjected to elevated temperatures. *Tunnelling and Underground Space Technology* 118:104170, DOI: 10.1016/j.tust.2021.104170
Shirato M, Furuichi K, Takimoto K, Hara H, Mukuno K, Yoshida K (2003) Development of new composite segment and application to the tunneling project. *Journal of JSCE* 728:157-174, DOI: 10.2208/jscej.2003.728_157 (in Japanese)
Talmon AM, Bezuijen A (2013) Calculation of longitudinal bending moment and shear force for Shanghai Yangtze River Tunnel: Application of lessons from Dutch research. *Tunnelling and Underground Space Technology* 35:161-171, DOI: 10.1016/j.tust.2013.01.001
Tan X, Chen W, Wu G, Wang L, Yang J (2020) A structural health monitoring system for data analysis of segment joint opening in an underwater shield tunnel. *Structural Health Monitoring* 19(4):1032-1050, DOI: 10.1177/1475921719876045
Tao L, Ding P, Lin H, Wang H, Wu S (2021) Three-dimensional seismic performance analysis of large and complex underground pipe trench structure. *Soil Dynamics and Earthquake Engineering* 150(2):106904, DOI: 10.1016/j.soildyn.2021.106904
Tao L, Ding P, Shi C, Wu X, Wu S, Li S (2019) Shaking table test on seismic response characteristics of prefabricated subway station structure. *Tunnelling and Underground Space Technology* 91:102994, DOI: 10.1016/j.tust.2019.102994
Tao L, Ding P, Yang X, Lin P, Zhao J (2020) Comparative study of the seismic performance of prefabricated and cast-in-place subway station structures by shaking table test. *Tunnelling and Underground Space Technology* 105:103583, DOI: 10.1016/j.tust.2020.103583
Tao L, Shi C, Ding P, Li S, Wu S, Bao Y (2022a) A study on bearing characteristic and failure mechanism of thin-walled structure of a prefabricated subway station. *Frontiers of Structural and Civil Engineering* 16(3):359-377, DOI: 10.1007/s11709-022-0816-2
Tao L, Shi C, Ding P, Yang X, Bao Y, Wang Z (2022b) Shaking table test of the effect of an enclosure structure on the seismic performance of a prefabricated subway station. *Tunnelling and Underground Space Technology* 125:104533, DOI: 10.1016/j.tust.2022.104533
Teachavorasinskun S, Chub-uppakarn T (2010) Influence of segmental joints on tunnel lining. *Tunnelling and Underground Space Technology* 25(4):490-494, DOI: 10.1016/j.tust.2010.02.003
Van Nguyen Q, Fatahi B, Hokmabadi AS (2017) Influence of size and load-bearing mechanism of piles on seismic performance of buildings considering soil-pile-structure interaction. *International Journal of Geomechanics* 17(7):4017007, DOI: 10.1061/(ASCE)GM.1943-5622.0000869
Wang Q, Geng P, Guo X, Zeng G, Chen C, He C (2021) Experimental study on the tensile performance of circumferential joint in shield tunnel. *Tunnelling and Underground Space Technology* 112:103937, DOI: 10.1016/j.tust.2021.103937
Wang S, Jiang X, Bai Y (2019) The influence of hand hole on the ultimate strength and crack pattern of shield tunnel segment joints by scaled model test. *Frontiers of Structural and Civil Engineering* 13(5):1200-1213, DOI: 10.1007/s11709-019-0546-2
Wang J, Liu H, Liu H (2018a) Measuring joint opening displacement between model shield-tunnel segments for reduced-scale model tests. *Structures* 16:112-118, DOI: 10.1016/j.istruc.2018.09.003
Wang X, Shi B, Wei G, Chen SE, Zhu H, Wang T (2018b) Monitoring the behavior of segment joints in a shield tunnel using distributed fiber optic sensors. *Structural Control and Health Monitoring* 25(1): e2056, DOI: 10.1002/stc.2056
Wood AMM (1975) The circular tunnel in elastic ground. *Géotechnique* 25(1):115-127, DOI: 10.1680/geot.1975.25.1.115
Wu H, Shen S, Chen R, Zhou A (2020) Three-dimensional numerical modelling on localised leakage in segmental lining of shield tunnels. *Computers and Geotechnics* 122:103549, DOI: 10.1016/j.compgeo.2020.103549
Yang M, Li H, Li N, Yang S (2020) Effect of subway excavation with different support pressures on existing utility tunnel in xi'an loess. *Advances in Civil Engineering*, DOI: 10.1155/2020/8818949
Zhang W, Koizumi A (2010) Behavior of composite segment for shield tunnel. *Tunnelling and Underground Space Technology* 25(4):325-332, DOI: 10.1016/j.tust.2010.01.007
Zhang W, Qi J, Zhang G, Niu R, Zhang C, He L, Lyu, J (2022a) Full-scale experimental study on failure characteristics of key segment in shield tunnel with super large cross-section, *Tunnelling and Underground Space Technology* 129:104671, DOI: 10.1016/j.tust.2022.104671
Zhang W, Zhang Q, Cao W (2021a) Study on stress and deformation of bolt joints of shield tunnel under static and seismic action. *KSCE Journal of Civil Engineering* 25(8):3146-3159, DOI: 10.1007/s12205-021-1339-4
Zhang G, Zhang W, Cao W, Wang B, Lai T, Guo W, Gao P (2021b) A novel test setup for determining waterproof performance of rubber gaskets used in tunnel segmental joints: Development and application. *Tunnelling and Underground Space Technology* 115:104079, DOI: 10.1016/j.tust.2021.104079
Zhang G, Zhang W, Li H, Cao W, Wang B, Guo W, Gao P (2021c) Waterproofing behavior of sealing gaskets for circumferential joints in shield tunnels: A full-scale experimental investigation. *Tunnelling and Underground Space Technology* 108:103682, DOI: 10.1016/j.tust.2020.103682
Zhang D, Zhang B, Luo T, Zhang D, Li B (2022b) Full-scale testing and numerical modelling of segmental-joint performance with corroded bolt. *Tunnelling and Underground Space Technology* 119:104260, DOI: 10.1016/j.tust.2021.104260
Zhou L, Zhu H, Shen Y, Guan L, Yan Z, Sun W, Li Y (2022) Full-scale experimental investigation on progressive failure characteristics of shield segmental lining connected through segmental joints containing ductile-iron joint panels. *Archives of Civil and Mechanical Engineering* 22(3):120, DOI: 10.1007/s43452-022-00438-0
Zhou L, Zhu H, Yan Z, Shen Y, Meng H, Guan L, Wen Z (2019) Experimental testing on ductile-iron joint panels for high-stiffness segmental joints of deep-buried drainage shield tunnels. *Tunnelling and Underground Space Technology* 87:145-159, DOI: 10.1016/j.tust.2019.02.009
Zuo L, Li G, Feng K, Ma X, Zhang L, Qiu Y, Cao S, Feng L (2018) Experimental analysis of mechanical behavior of segmental joint for gas pipeline shield tunnel under unfavorable compression-bending loads. *Tunnelling and Underground Space Technology* 77:227-236, DOI: 10.1016/j.tust.2018.03.005